Published in final edited form as:
Mol Microbiol. 2011 July ; 81(1): 192–205. doi:10.1111/j.1365-2958.2011.07688.x.

The SLH-domain protein BslO is a determinant of *Bacillus anthracis* chain length

Valerie J. Anderson, **Justin W. Kern**, **Justin W. McCool**, **Olaf Schneewind**, and **Dominique Missiakas**[*]
Department of Microbiology, University of Chicago, Chicago, IL 60637, USA

Summary

The Gram-positive pathogen *Bacillus anthracis* grows in characteristic chains of individual, rod-shaped cells. Here, we report the cell-separating activity of BslO, a putative *N*-acetylglucosaminidase bearing three N-terminal S-layer homology (SLH) domains for association with the secondary cell wall polysaccharide (SCWP). Mutants with an insertional lesion in the *bslO* gene exhibit exaggerated chain lengths, though individual cell dimensions are unchanged. Purified BslO complements this phenotype *in trans*, effectively dispersing chains of *bslO*-deficient bacilli without lysis and localizing to the septa of vegetative cells. Compared to the extremely long chain lengths of *csaB* bacilli, which are incapable of binding proteins with SLH-domains to SCWP, *bslO* mutants demonstrate an chaining phenotype that is intermediate between wild-type and *csaB*. Computational simulation suggests that BslO effects a non-random distribution of *B. anthracis* chain lengths, implying that all septa are not equal candidates for separation.

Introduction

The Gram-positive, zoonotic pathogen *Bacillus anthracis* is the causative agent of anthrax (Koch, 1876). The organism exists in two distinct forms: vegetative, rod-shaped bacilli and smaller, oblong endospores (Koch, 1876). Following spore entry into a new host, the microbe germinates and its vegetative forms disseminate to all organ tissues (Koch, 1876). Two features enable vegetative bacilli to evade clearance by host phagocytes, the elaboration of a thick capsule comprised of poly-γ-D-glutamic acid (PDGA) and the ability to form chains of bacilli that are tethered end-to-end at their septal peptidoglycan (Bruckner *et al*., 1953, Preisz, 1909). Chains of bacilli, which microscopically resemble bamboo shoot-like filaments, present a physical obstacle for engulfment by immune cells (Ruthel *et al.*, 2004, Dixon *et al*., 2000). The envelope of *B. anthracis* is a complex matrix of peptidoglycan covalently decorated with secondary cell wall polysaccharide (SCWP), proteins and a poly-D-γ-glutamic acid (PDGA) capsule (Fouet, 2009). In addition, *B. anthracis* elaborates a surface layer (S-layer): a self-assembling paracrystalline layer of protein (Mesnage *et al*., 1998). In non-encapsulated bacilli, such as those from the vaccine strain *B. anthracis* Sterne (Sterne, 1937), the Slayer constitutes the topologically outermost surface (Mesnage et al., 1998). In *B. anthracis*, retention of S-layers occurs through a non-covalent interaction of the conserved SLH-domains triplet sequence with the pyruvylated SCWP (Mesnage *et al*., 2000, Kern *et al.*, 2010).

Bacterial peptidoglycan hydrolases (PH) are enzymes that cleave bonds within the murein sacculus, a macromolecule composed of glycan strands with the iterative disaccharide (*N*-acetylmuramic acid-(β1–4)-*N*-acetylglucosamine) crosslinked by wall peptides(Strominger

[*]For correspondence: 920 East 58th Street, Chicago, IL 60637, USA; dmissiak@bsd.uchicago.edu; Tel: 773 834 8161; Fax: 773 834 8150.

& Ghuysen, 1967, Shockman & Holtje, 1994). PHs can have very specific functions, such as peptidoglycan hydrolysis during germination and sporulation or flagellar assembly, as well as the generic maintenance of cell wall structural homeostasis. Because excessive hydrolysis of the murein sacculus compromises cell wall integrity, the activity of these enzymes must be strictly regulated to prevent autolysis (Shockman & Holtje, 1994). Depending on the substrate specificity of the enzyme, PHs can hydrolyze glycosidic, amide or peptide bonds to disassemble the peptidoglycan (Ghuysen, 1968). Thus, PHs can be classified as *N*-acetylmuramyl-L-alanine amidases, endopeptidases, carboxypeptidases, *N*-acetylmuramidases, lytic transglycosylases and *N*-acetylglucosaminidases (Vollmer *et al.*, 2008). The functional assignment of individual enzymes to specific physiological roles in cell wall morphogenesis is often stymied for two reasons; first, most bacterial genomes encode for multiple PHs, indicative of functional redundancy, and second, PHs may serve multiple functions, such as cell wall turnover and daughter cell separation (Smith *et al.*, 2000).

The majority of published data on *B. anthracis* PHs focus on germination-specific lytic enzymes that cleave cortex substrates containing muramic-δ-lactam residues (Dowd *et al.*, 2008, Heffron *et al.*, 2010, Heffron *et al.*, 2009). With respect to vegetative bacilli, *in vitro* analysis of a few recombinant, purified proteins demonstrated murein hydrolytic activity for the prophage endolysin PlyL (Low *et al.*, 2005)and three proteins with SLH-domains: AmiA (Mesnage & Fouet, 2002), Sap and EA1 (Ahn *et al.*, 2006). How PHs act on *B. anthracis* vegetative forms *in vivo* and whether such enzymes contribute to the chaining phenotype of this microbe has not yet been studied. Recent work on other microbes identified PHs that cleave the septa between daughter cells as the last step of cell division. Mutations that abrogate the expression of these enzymes are affiliated with a chaining phenotype in *Lactococcus lactis* (*acmA*) (Buist *et al.*, 1995), *Listeria monocytogenes* (*murA*) (Carroll *et al.*, 2003)and *Escherichia coli* (*amiA, amiB,* and *amiC*) (Heidrich *et al.*, 2001)or a clustering phenotype in *Staphylococcus aureus* (Sugai *et al.*, 1995). Here we asked whether similar mutants can be isolated for *B. anthracis*.

Results

Bacillus anthracis variants with chain length phenotypes

To identify variants with increased chain length, we employed random mutagenesis with the *bursa aurealis* transposon to create *B. anthracis* Sterne variants (Tam *et al.*, 2006). To assess the morphology of bacilli, flow cytometry forward scatter (FSC) and side scatter (SSC) parameters were used as proxies for relative cellular volume and refractivity, respectively (Allman *et al.*, 1992, Bouvier *et al.*, 2001). By comparing mean FSC-A and SSC-A signals (N = 10,000 events per strain), we identified several mutants, one of which produced dramatically increased forward scattering relative to an age-matched wild-type control (3.9062e3 versus 1.2171e3). Inverse PCR mapped the transposon insertion within *bas1683*, a gene specifying a 459 amino acid translational product (Fig. 1A). A recent report identified this ORF as a member of a group of SLH-domains containing proteins, naming it *bslO* (*b*acillus *s*urface *l*ayer *O*)(Kern & Schneewind, 2008).

Characterization of the *bslO* phenotype using flow cytometry

The domain architecture of BslO predicts a Gram-positive, cleavable signal peptide (Bendtsen *et al.*, 2004), three SLH-domains and a putative glucosaminidase domain (PF01832) (Finn *et al.*, 2010). Two linker regions, L1 and L2, separate the putative glucosaminidase domain from the SLH-domains and the C-terminus of the protein, respectively (Fig. 1A). Glucosaminidases cleave peptidoglycan strands at the glycosidic β(1→4) bond between GlcNAc and MurNAc. Because glucosaminidases of other bacteria,

for example *S. aureus* Atl (Oshida *et al.*, 1995)and *S. pneumoniae* LytB (De Las Rivas *et al.*, 2002), are known to contribute to bacterial separation *in vivo*, we sought to characterize the phenotype of the *bslO* mutant strain.

Flow cytometry was used to compare *bslO* and wild-type bacilli at multiple time points during vegetative growth. The greatest differences between *bslO* and control FSC distributions occurred during exponential phase; the linear least-squares slope of the *bslO* versus Sterne FSC data was greatest three hours after spore suspension into rich medium (Fig. 1BC). Flow cytometry data for the *bslO* mutant revealed consistently larger FSC-A ranges as compared to Sterne, with a subpopulation of events displaying relatively high SSC and FSC values (FSC-A $>10^3$ and SSC-A $>10^4$) (Fig. 1B). This observation could be explained if the *bslO* mutation deregulated the size of bacilli, yielding a more variable FSC distribution overall or longer chains of vegetative forms than the parent strain Sterne (Fig. 1C).

Morphological phenotypes of *bslO* mutants

Visualized by light microscopy, the margins of *B. anthracis* Sterne colonies appeared as contours of ordered, closely-packed chains of bacilli that curve in unison (Fig. 2A). In contrast, the edges of *bslO* colonies appeared disaggregated, with large intervening gaps between chains that jutted out from the colony in angular points (Fig. 2A). Viewed by transmission electron microscopy of thin-sectioned bacilli, the morphology of individual *bslO* mutant or Sterne parent cells did not display differences in cell dimension, cell wall thickness or septal morphology (Fig. 2A). Fluorescent microscopy experiments examining the dimensions and distributions of membranes and chromosomes in bacilli did not reveal differences between wild-type and *bslO* mutant bacilli (*vide infra*), suggesting that the *bslO* mutation appears to impact only the chain length of *B. anthracis*.

When grown in liquid media, *bslO* culture turbidity was non-homogeneous during exponential phase growth, as though cells had aggregated. Following centrifugation, the sedimentation pellets of *B. anthracis* Sterne cultures were well-compacted, where as those of *bslO* mutants were loose, even after repeat centrifugation (Fig. 2B). Light microscopy of exponential-phase bacteria showed a length phenotype among *bslO* mutants; mutant bacilli were approximately 4-fold longer than their parent (Fig. 2C). A significant population of short *bslO* chains was not observed, which is what one might expect if the *bslO* mutation deregulated, rather than increased, overall chain length.

Role of bslO and growth phase of the chain lengths of bacilli

To measure growth and chain length of bacilli, spore preparations were suspended into fresh media and monitored for changes in optical density (A_{600nm}) over time (Fig. 3A). The growth curves appeared super-imposable between strains, implying that BslO is dispensable for replication (Fig. 3A). At indicated time points, production of BslO was assayed by immunoblot (Fig. 3B) and a corresponding aliquot was fixed for measuring chain lengths by light microscopy (Fig. 3CD). An immunoblot of total culture preparations collected over time revealed BslO production as early as 1 h after dilution of bacilli into rich media and at all subsequent time points (Fig. 3B). *B. anthracis* Sterne chains lengthened significantly in lag phase (1–2 h) (Fig. 3C). Chain lengthening continued into early exponential phase (3–4 h), but subsequently the filaments shortened. The chains of *bslO* bacilli looked virtually identical to Sterne cells during lag phase (Fig. 3C). Subsequently, *bslO* chains were dramatically longer than their wild-type parent. To compare chain lengths quantitatively, we measured the chain lengths of individual bacilli ($N = 100$ chains) from light micrographs (Fig. 3D). The average chain length of *B. anthracis* Sterne was measured as 32.22 (±11.23 S.D., n=100) μm, that of the *bslO* mutant as 60.77 (±30.82) μm. Manifestation of a *bslO*

length phenotype was coincident with the culture's entry into exponential growth phase (3 h) (Fig. 3D).

Cis and trans complementation of *bslO* mutant phenotypes

A plasmid (p*bslO*) encoding the wild-type *bslO* allele under transcriptional control of the IPTG-inducible P_{spac} promoter was transformed into the *bslO* mutant strain. Growth of the genetically-complemented *bslO* strain in the presence, but not the absence, of IPTG restored the compaction of cell pellets upon centrifugation, similar to those of *B. anthracis* Sterne (Fig. 4A). Light micrographs of bacilli grown in the presence of IPTG showed that *bslO* cells transformed with the complementing vector displayed chain lengths more comparable to those of Sterne, rather than *bslO* bacilli (Fig. 4B). Chain length data were compiled as before, verifying that plasmid-based expression of *bslO* enhanced cell separation comparable to that of wild-type bacilli(Fig. 4C). Immunoblots of total culture preparations confirmed that BslO was synthesized only in the presence of the inducer in the complemented strain, and never in vector control transformants (Fig. 4D).

Recombinant BslO (rBslO) or a fusion protein with maltose-binding protein (rMBP-BslO) were expressed and purified from *E. coli* (Fig. S1). When added to *bslO* mutant bacilli, rBslO or rMBP-BslO demonstrated comparable chain dispersing activity, indicating that the amino terminal addition of MBP to rBslO did not affect BslO function (Fig. S1). Bacilli incubated with rBslO were shorter than mock-treated controls, independent of the genotype (Fig. 4EF). When either *bslO* or wild-type parent cells were incubated with rBslO, the median chain length converged to approximately 10–20 μm at 2 μg per 10^7 bacilli (Fig. 4E). Using an empirically-determined mean cell length as determined by FM4–64 staining (4.61 μm, ±1.43 μm (S.D.), $N = 100$), we estimated that the majority of bacilli consist of two to six cells per chain at saturating concentrations of rBslO (Fig. 4E). Thus, not only did extracellular rBslO complement the chaining phenotype of *bslO* mutants, but we also found that endogenous BslO activity was not saturated, as Sterne chains could be shortened beyond wild-type lengths to the same apparent minimum length.

B. anthracis spores were suspended in fresh media and cultures were incubated in the presence of either rBslO or rPlyL, the lambda prophage Ba02 endolysin (Low et al., 2005). While the optical density of cultures treated with rBslO increased with time, the optical density of PlyL-treated cells declined with increasing concentrations of the enzyme (Fig. S2). Thus, additions of large amounts of rBslO, with or without the MBP fusion, did not lyse bacilli.

BslO-mCherry and rBslO localize to cell septa

To observe BslO localization on the surface of vegetative bacilli, *B. anthracis* Sterne was mutated to express the translational hybrid BslO-mCherry, replacing wild-type BslO (Fig. 5A). The length distributions of BslO-mCherry expressing bacilli were equivalent to those of its wild-type parent, implying that BslO-mCherry was functional (data not shown). As a control, *B. anthracis* was mutated to express a translational hybrid between the surface array protein (Sap) and mCherry (*sap-mcherry*) (Fig. 5A). Sap is the major S-layer protein enveloping bacilli during exponential growth (Mignot *et al.*, 2002). Bacilli expressing *bslO-mCherry* displayed faint, diffuse staining throughout the envelope and puncta of bright fluorescence coincident with cell septa (Fig. 5B). In contrast, bacilli expressing *sap-mCherry* displayed contiguous areas of intense fluorescence interrupted by non-fluorescent patches somewhat randomly arrayed over the chain (Fig. 5C). A fraction of Sap-mCherry was also located at the poles of some vegetative cells. Pixel intensity distributions of transects spanning the major axis of individual cells were analyzed for each strain. To account for cell-to-cell variations in protein expression and length, raw pixel intensities and

transect lengths were measured and normalized with ImageJ (Abramoff *et al.*, 2004). Transect plots revealed a distinct polar distribution of BslO-mCherry as pixel intensities increased away from the midcell (0.5) (Fig. 5D). By comparison, the intensity transects of Sap-mCherry appeared random at cell-level resolution (Fig. 5D). As BslO-mCherry localized to the septa of vegetative forms, we wondered whether the same was true for rBslO added at a concentration of 5 μg mL^{-1} to the extracellular media of cultures (Fig. 5E). rBslO conjugated to Alexafluor 488 (Invitrogen) bound all *bslO* cells examined. In some cases (~ 25% of total cells examined), rBslO was uniformly-distributed in the envelope of bacilli, including the septa that connect cells within *B. anthracis* chains. Nevertheless, for the majority of bacilli rBslO was deposited at or near the septa (Fig. 5E).

BslO treatment of *csaB* mutant bacilli

Mutants that lack *csaB* (cell surface attachment B) cannot pyruvylate SCWP and fail to assemble S-layers or incorporate SLH-domain proteins into the envelope of *B. anthracis* (Mesnage et al., 2000, Kern et al., 2010). Fouet proposed that the *csaB* phenotype results from the inability of mutants to assemble S-layers or bind SLH-domain proteins that contribute to cell separation, specifically those with PH domains (Fouet, 2009). If so, the composite phenotype of *csaB* mutants may be derived from the functional losses of several factors with SLH-domains. In contrast, the phenotype of *bslO* variants could be viewed as an intermediate between the chaining pattern of wild-type bacilli and *csaB* mutants. We performed chain length analyses for wild-type, *csaB* and *bslO* strains (Fig. 6A). Within two hours of dilution spores into fresh media, all three strains displayed similar length distributions. By three hours, *bslO* and *csaB* length distributions were comparable, though the median chain length of each mutant was 4 or 5-fold longer than that of Sterne bacilli (Fig. 6A). By four hours, *csaB* bacilli continued to lengthen and the median length exceeded the 75^{th} percentile of *bslO* chain lengths (288.83 μm versus 336.49 μm, Fig. 6A). While chain lengths of all strains shortened as they entered early stationary phase, the median chain length recorded for *csaB* chains was about 12-fold longer than the Sterne control (10.02 μm versus 126.32 μm). Thus, the chaining phenotype of *bslO* variants was not as pronounced as that of *csaB* mutants.

To verify that *csaB* mutations do not impact BslO expression, protein samples derived from *B. anthracis* Sterne or its *bslO* and *csaB* variants were analyzed by immunoblotting (Fig. 6B). Further, we determined that the lengths of individual cells, as opposed to chain lengths, were equivalent between Sterne, *bslO* and *csaB* bacilli (Fig. 6C and Fig. S3). Fluorescence microscopy of dual-stained bacilli with FM4–64 (membrane) and Hoechst (DNA) indicated that individual cells completed cell division with proper chromosomal partitioning (Fig. 6C). We therefore conclude that *bslO* and *csaB* mutants are defective for chain separation, not cell septation, and that *csaB* variants are also arrested at this final step of the division cycle for *B. anthracis* vegetative forms. Thus, a full complement of SLH-domain PHs may be necessary to achieve efficient cell separation of *B. anthracis* chains.

We were intrigued by the observation that AmiA, another SLH-domain PG hydrolase, could hydrolyze *csaB* cell wall peptidoglycan in zymograms, indicating its catalytic activity may be uncoupled from its ability to bind the envelope (Mesnage & Fouet, 2002). If *csaB* bacilli secrete SLH-domain hydrolases into the supernatant, as they do with Sap and EA1, the reduced capacity of *csaB* mutants to separate may be due to the reduced local concentration of these proteins at the cell surface. Thus, if recombinant BslO were supplied in excess, *csaB* chain lengths might be reduced even though the protein cannot bind the envelope via its SLH-domains. To test this, exponential phase *csaB* cultures were split into aliquots and incubated for 1 h with rBslO, which revealed a dose-dependent shortening of mutant bacilli (Fig. 6D). While *csaB* lengths tended to converge at high concentrations (100–200 μg mL^{-1}), the median value remained 2-fold that of Sterne or *bslO* lengths, *i.e.* 26.83 μm

versus 12.33 μm and 15.16 μm, respectively (Fig. 6D and Fig. 4E). Nevertheless, *csaB* mutants eventually appeared resistant to further shortening at the highest rBslO concentrations (Fig. 6D). Consequently, the range of lengths observed at 200 μg mL^{-1} of rBslO was much greater in *csaB* samples (~ 320 μm) than in *bslO* (32 μm) or Sterne samples (25 μm, Fig. 6D and Fig. 4E). Together these data suggest that the association of BslO SLH-domains with SCWP may bean important contributor but not absolutely essential for its activity.

To further test the contribution of SLH-domains to BslO function, a competition experiment was devised. *bslO* bacilli were incubated with a fixed amount of rBslO and the purified, recombinant SLH-domains of BslO at various ratios (Fig. 6E and Fig. S4). At the lowest ratio tested (1 SLH-domain:100 rBslO), the chain lengths were indistinguishable from those of a rBslO-only control suspension. However, addition of the SLH-domains in as little as one tenth the concentration of full length protein reduced the apparent activity of rBslO in a dose-dependent manner (Fig. 6E).

Model for BslO-dependent separation of *B. anthracis* chains

Micrographs of bacilli show chains with varying degrees of constriction at cell wall septa, with deeper invaginations at septa spaced 4–8 cells apart (Fig. S5). Close inspection of rBslO-treated chains revealed a decrease in mean chain length as compared to untreated bacilli, yet measured distributions suggested bacilli separated into daughters of relatively uniform length (Fig. 4F). We hypothesized that such distribution cannot occur if each septum was equally susceptible to rBslO cleavage. A Monte Carlo approach was used to model BslO cleavage of cell septa. *B. anthracis* cell and chain lengths in the presence or absence of rBslO were empirically determined by microscopy. A Weibull distribution was used to simulate chain length populations fitted to the observed populations of uncut chains of bacilli (Fig. S6). We next estimated the number of individual cells in a given chain drawing from a Poisson distribution fitted to the observed cell length data. Next, we established rules to simulate rBslO-mediated cell separation and tested the validity of these rules by comparing the mean histogram of 10,000 simulations to the empirical distribution of chain lengths that had been treated with 2 μg rBslO (Fig. 7).

Three types of rules were explored. First, cells drawn randomly from the population were separated at a randomly selected septum (Fig. 7A). The results showed that no matter how many cuts were applied to the initial population, the resultant distribution did not match the observed distribution. Specifically, these simulations suggested that, were rBslO to act in a random fashion, one would observe higher frequencies of very short chains and very long chains; this was not observed *in vivo*. In a second model, selected chains were cut it in half, or approximately in half for chains with odd numbers of cells (Fig. 7B). While this model fit the observed data better than a random cleavage model, it still simulated distributions biased toward producing higher frequencies of short-chained bacilli. The third model introduced two rules simultaneously: chains with fewer than eight cells are never candidates for cleavage, and the minimal daughter chain comprises three cells on average (Fig. 7C). The minimum daughter lengths were not mathematically-optimized; rather, we arrived at this set by trial-and-error, because simulations run employing a single length minimum (e.g. 2 cells long) did not fit the observed data very well. The two-rule model simulated the observed distribution more closely than the two earlier models. In some of its simulations, the candidate pool (chains with more than seven cells) was exhausted prematurely after more than 75 rounds of cutting, as each Monte Carlo simulation has a unique starting distribution and a finite number of chains longer than 7 bacilli. For illustration, we included a scenario with 90 cuts and collected 10,000 valid simulations. At this frequency, a small number of simulations (~1–2% of the total runs) were invalid: the starting population did not include enough chains to be cut 90 times). Thus, although two-rule simulation introduced a bias that

favored starting distributions with greater frequency of long chains, a sufficient number of simulations were generated so as not to cause significant alteration of the underlying distribution. That the two-rule, minimum length model most closely reproduced the experimental chain length distributions and the observation that septa displayed varying degrees of constriction (*vide supra*) might suggest that cell septa develop over a time interval longer than the cell cycle that eventually ends in BslO-mediated cleavage.

Discussion

The attribute of *B. anthracis* to form chains of vegetative cells is thought to contribute to its ability of resisting opsono-phagocytic killing by immune cells(Ruthel et al., 2004). We used flow cytometry to quantify chain length during *B. anthracis* vegetative growth. Upon dilution into growth media, *B. anthracis* chains initially increased in length. This increase gradually declined until bacilli assumed chain lengths observed in stationary phase cultures. A screen for *B. anthracis* mutants with increased chain length identified an insertional mutation in *bslO*. BslO is a secreted polypeptide with N-terminal SLH-domains and C-terminal predicted *N*-acetylglucosaminidase domain. Following signal peptide cleavage, the mature protein is retained in the envelope, which is likely a consequence of the binding of SLH-domains to pyruvylated SCWP (Kern et al., 2010). BslO is one of twenty-two S-layer associated polypeptides encoded in the *B. anthracis* genome (Kern & Schneewind, 2008). Unlike BslA, an S-layer associated polypeptide distributed throughout the envelope of bacilli (Kern & Schneewind, 2008, Kern & Schneewind, 2009), BslO accumulates near the septum. Trafficking of BslO to the septum likely contributes to its function, the cleavage of septal peptidoglycan, as *bslO* mutants are defective in the release cells from growing *B. anthracis* chains.

Computational simulations suggest that the selection of septa for BslO cleavage occurs by a non-random process. *In vivo* rules governing *B. anthracis* chain length are likely simple and emergent from biological properties like septum age and growth rate. We favor a model of *B. anthracis* cell separation whereby septation is completed during each division cycle, however septum maturation requires additional rounds of cell division before it can be cleaved. Perhaps this lag is reflective of the recruitment time for the proper enzymes to fully catalyze peptidoglycan hydrolysis. Because *bslO* variants display an intermediate chain-formation phenotype between *csaB* mutant and wild-type strains, we hypothesize that other PHs with SLH-domains may contribute to cell wall homeostasis.

Muralytic enzymes that complete the bacterial cell cycle by separating daughter cells have been described for other Gram-positive microbes. *Staphylococcus aureus* secretes the hybrid *N*-acetylglucosaminidase/amidase Atl as well as the amidase Sle1 (Oshida et al., 1995, Kajimura *et al.*, 2005). Repeat domains direct Atl to the septa(Baba & Schneewind, 1998), whereas the N-terminal LysM domain of Sle1 is thought to promote interaction with septal peptidoglycan (Kajimura et al., 2005). The specific feature of *S. aureus* peptidoglycan that attracts Atl and Sle1 to the septa is not known. However, without such positional information staphylococci cannot separate their cells. Similarly, *atl* or *sle1* staphylococci accumulate large clusters of cells that cannot separate. *Lactococcus lactis N*-acetylglucosaminidase AcmA, *Listeria monoctogenes N*-acetylmurmidase MurA (Carroll et al., 2003)and *Enterococcus faecalis N*-acetylglucosaminidase AtlA (Mesnage *et al.*, 2008)fulfill analogous functions and separate daughter cells by cleaving septa. All three enzymes harbor LysM domains that are thought to provide positional information(Steen *et al.*, 2005). In contrast, the genome of *B. anthracis* does not encode secreted proteins with LysM domains(Read *et al.*, 2003). We presume proper positioning of BslO in *B. anthracis* is achieved through its SLH-domains and the interaction with SCWP and S-layer proteins.

Experimental procedures

Bacterial strains and growth conditions

B. anthracis Sterne 34F2 and its variants were cultured in Luria broth (LB) at 37 °C or 30 °C when using pLM4 or pLM5-based vectors (Marraffini & Schneewind, 2006). *E. coli* DH5α, K1077 and BL21 (DE3) were grown in LB. Media were supplemented with spectinomycin (200 μg ml^{-1}), tetracycline (5 μg ml^{-1}) or kanamycin (20 μg ml^{-1}) to maintain plasmid selection in *B. anthracis* or kanamycin (50 μg ml^{-1}) and ampicillin (100 μg ml^{-1}) in *E. coli. B. anthracis* strains were sporulated using modified G medium (modG) as described(Kim & Goepfert, 1974). Spore suspensions were germinated by inoculation into LB and grown at 37 °C unless otherwise noted.

DNA manipulations and plasmids

Plasmid DNA used to transform *B. anthracis* was purified from *E. coli* K1077 (*dcm*$^{-}$/*dam*$^{-}$) (Fulford & Model, 1984). Plasmid p*bslO* used for complementation studies was made by PCR amplification of the *bslO* open reading frame genomic DNA using primers *bslO*F and *bslO*R followed by cloning in the pLM5 vector. The fluorescent translational hybrid was created via allelic replacement using vector pLM4. Two fragments of approximately 1 kb DNA sequences flanking the *bslO* TAA stop codon were amplified by PCR (using two primers pairs *bslO-mcherry* UPF, *bslO-mcherry* UPR and 3′ *bslO-mcherry* DNF, *bslO-mcherry* DNR) and cloned into pLM4 to generate plasmid p*bslO*KO. In this construct, a *Kpn*I restriction site was inserted right before the the *bslO* TAA stop codon and used to insert a PCR fragment encoding a *Kpn*I-flanked *mcherry* sequence generated with primers P283 and P284 yielding plasmid p*bslO-mcherry*. Allelic replacement using p*bslO-mcherry* was performed as previously described(Marraffini & Schneewind, 2006). The transcriptional hybrid between *sap* and *mcherry* was achieved using an identical approach using primers P293, P294, P303, and P304. rBslO was expressed from pMCSG19 transformed in *E. coli* BL21 (DE3)(Donnelly *et al.*, 2006). The *bslO* open reading frame was amplified by PCR with primers *bslO*-LICF and *bslO*-LICR and inserted into pMCSG19 using ligation-independent cloning as previously described(Donnelly et al., 2006). BslO purified without the MBP was expressed from the same construct in *E. coli* BL21 (DE3) harboring pRK1037. The SLH-domains of BslO were amplified using oligos $bslO_{SLH}$F and $bslO_{SLH}$R and cloned into pET-16B (Novagen). Recombinant PlyL was expressed from apET-16B-derived plasmid pJB1 and produced as previously described (Marraffini & Schneewind, 2007). Primers used in this study are listed in Table 1. Transposon mutagenesis was carried out using *bursa aurealis* mutagenesis (Tam et al., 2006). The location of transposon insertions was determined by extracting chromosomal DNA using the Promega Genomic Wizard kit. Sequence analyses of inverse PCR products of the transposon/chromosome junction were performed with the primers Martn-F and SpecR (Tam et al., 2006).

Flow cytometry analysis

Bacilli were sporulated, purified and then germinated in 3 ml LB at 37 °C to temporarily synchronize the growth of a population of vegetative cells. Aliquots (0.5 ml) were fixed via the addition of buffered formalin, diluted to a maximal absorbance (A_{600nm}) of 0.1 and subjected to flow cytometry using a LSR II (BD Biosciences). Optical pulse FSC-A and SSC-A parameters were collected, gating on signals larger than those observed for suspensions of fixed, non-viable spores for N = 10,000 events. Subsequent files were analyzed using custom scripts in Matlab and the FCS data reader function. Data presented are representative of 1 at least 2 biological replicates.

Light and fluorescence microscopy

Samples subjected to light microscopy were fixed with addition of buffered formalin (4% final volume) and observed on glass slides and cover slips. Digital micrographs of fixed samples were collected on an Olympus PROVIS microscope with 100×, 60× or 40× objectives or a Zeiss Axioplan 2 microscope using 63× or 100× objectives, both equipped with a CCD camera (Hamatsu Orca or Andor Technology, respectively). To account for bacilli whose lengths extended beyond that of the camera's field of view, images were tiled using Photoshop 6.0 (Adobe). Micrographs of colonies were collected by visualizing LB agar plates streaked with *B. anthracis* and placed directly onto the stage. Length data were measured directly from micrographs in Photoshop 6.0 (Adobe). Fluorescent transects were calculated with the line segment tool in ImageJ (Abramoff et al., 2004)and transect normalization and plotting performed by custom scripts in Matlab R2009a (Mathworks). Length data were normalized by transforming the distance range to increments of 1 divided by the number of pixels along the transect. Fluorescent intensities were normalized by dividing observed intensity by the maximum intensity value recorded over the population of cells. Individual cell lengths were determined by measuring the major axis of live, mid-log bacilli that were incubated with FM4–64 at 10 μg mL^{-1} (membrane stain) and Hoechst at 10 μg mL^{-1} (DNA stain) at room temperature for 5 min, followed by 3 washes in LB. Data are representative of 1 of 2 biological replicates.

Electron microscopy

B. anthracis Sterne orits *bslO* variant were germinated in LB 37 °C for 4 hours. Vegetative forms were sedimented by centrifugation (8,000 ×*g*), washed three times in 0.1 M sodium cacodylate, pH 7.4 and then fixed for 2 h in the same buffer supplemented with 2% glutaraldehyde and 45% paraformaldehyde (vol/vol). After fixation, samples were washed three more times in the 0.1 M sodium cacodylate, stained, dehydrated and embedded for electron microscopy. 90 nm sections were examined at 300 KV with a FEI Tecnai F30 microscope equipped with a Gatan CCD camera.

Protein purification and antibody production

rBslO was produced in *E. coli* BL21 (DE3) transformed with pMCSG-*bslO* (Donnelly et al., 2006). *In vivo* cleavage of MBP from fusion proteins was achieved by transforming pMCSG-bslO into *E. coli* BL21 (DE3) harboring pRK1037. This plasmid produces the TVMV protease but not the Tet repressor (Donnelly et al., 2006). Recombinant PlyL was purified as described (Marraffini & Schneewind, 2007). Overnight cultures were refreshed 1:100 in LB and incubated at 30 °C until they reached an optical density of 0.5 A_{600nm} at which time IPTG (Fisher) was added to the culture to a final concentration of 1 mM and incubated for 4 h longer. Cells were sedimented by centrifugation, suspended in 50 mM Tris-HCl, 150 mM NaCl, 5% glycerol and frozen at −20 °C overnight. Cell pellets were then thawed and lysed in a French pressure cell (Thermo). The crude lysate was centrifuged and the filtered supernatant was subjected to affinity purification. His-tagged proteins were purified and concentrated on a Ni-NTA agarose affinity column by gravity flow and eluted with 250 mM imidazole. BslO purified without its MBP for activity assays and Alexafluor conjugates was purified by FPLC on an Akta Purifier (Pharmacia Biotech) over a Ni-NTA Superflow column (Qiagen), dialyzed in 2L 20 mM Tris-HCl/5% glycerol pH 7.6 for 2 h at 4 °C in a Spectrapore #7 membrane, and then subjected to anion exchange chromatography over a HiTrap SP column (Pharmacia Biotech) eluting with NaCl. Pooled protein fractions were concentrated by sucrose dialysis and dialyzed 2 × 12 h in 5 mM sodium phosphate buffer with 5% glycerol, pH 7.5. To purify the SLH-domains of *bslO*, the insoluble portion of the crude French-pressed lysate was dissolved in Buffer A (6 M guanidine-HCl, 10 mM Tris-HCl, 100 mM NaH_2PO_4, pH 8.0) and applied to a gravity flow column packed with Ni-NTA agarose beads. The column was washed with 2 column volumes of Buffer A, followed

by 2 column washes with 50 mM Tris-HCl, 150 mM NaCl, 5% glycerol and then eluted. Purified SLH-domains were dialyzed to remove imidazole and subjected to a second round of Ni-NTA purification with the FPLC as described above. Protein concentrations were determined via BCA Assay (Pierce) and samples stored at −20 °C or −80 °C. Aliquots of rBslO were dialyzed in a Spectrapore #7 membrane into PBS, pH 7.5 at 4 °C for 4 h to remove primary amines from the buffer that might interfere in the Alexafluor488 conjugation. Alexa-BslO was labeled using the Alexa Fluor 488 Microscale Protein Labeling Kit (Invitrogen).

Specific antisera were generated by emulsifying 50 μg of purified, recombinant protein, dissolved in 500 μL of PBS with 500 μL of complete Freund's adjuvant (Difco) by sonication and subcutaneous inoculation of female New Zealand white rabbits. Two subsequent boosts were performed by emulsifying protein with incomplete Freund's adjuvant. Serum was harvested by cardiac puncture and stored at −80°C with 0.02% sodium azide.

Immunoblotting

To assess production of BslO by newly germinated bacilli as a function of growth, aliquots of cultures were collected at indicated time points using a cell volume equivalent to 5.0 A_{600nm}. Cells from bacterial pellets were disrupted using a FastPrep FP120 bead-beater (Thermo) and 0.1mm glass beads (BioSpec). Proteins in these suspensions were precipitated by addition of 10 % final concentration trichloroacetic acid, washed in cold acetone, solubilized in 100 μl of 0.5 M Tris-HCl (pH 8.0), 4% SDS and heated at 90 °C for 10 min. Proteins were separated on SDS-PAGE and transferred to poly(vinylidene difluoride) membrane for immunoblot analysis. Proteins were detected with specific rabbit polyclonal antibodies raised against purified protein at a dilution of 1:5,000 (αBslO) or 1:4,000 (αL6). Immunoreactive products were revealed by chemiluminescent detection after incubation with an anti-rabbit HRP-conjugate secondary antibody (1:20,000, Cell Signaling Technology).

Length distribution simulations

Custom scripts were written in Matlab R2009a (Mathworks). First, the major axis of 100 Sterne cells stained with FM4–64 were measured (pixels) in ImageJ. The lengths were converted to lengths in microns using a reference image of an objective micrometer (Nikon). The Matlab *poissfit* function returned the MLEλ Poisson parameter and the 95th percentile confidence interval (CI). λ was simulated drawing from a normal distribution (mean λ) and used to simulate a Poisson distribution of cell lengths by the *poissrnd* function for 1000 iterations (Fig. S6). For each chain, cell lengths drawn from the Poisson distribution are cumulatively-summed until they approximate the total chain length, thereby converting the length data into cells per chain. Chains treated with 2 μg rBslO are converted to cells per chain 1000 times using this process and the mean frequency histogram is presented as the observed data against which cleavage models are compared (Fig. 7, Fig. S7, red curve). The starting or 'uncut' bacilli chain lengths are simulated in the same method as the cell lengths using a Weibull distribution in which the distribution parameters are fitted to 100 measured chain lengths of *bslO* bacilli mock-treated with enzyme (Fig. S6). All simulations then follow a generic method: 100 bacilli lengths are simulated by the Weibull distribution. Each chain is individually-converted to cells per chain using the Poisson distribution. The probability of selecting a given chain is adjusted proportionate to its length to weight for numbers of septa. A cell is selected randomly. The chain containing the selected cell is separated according to a set of rules to create 2 daughter cells. The daughter cells replace the original cell in the original population to replace the mother cell. The process is repeated for a defined number of iterations. Each round of cutting increases the original population size

by 1 chain, e.g. 2 rounds of cutting increase the master pool from 100 chains to 102 chains. 100 chains are randomly selected from the population and the mean histogram is generated after 10,000 simulations. This replicates our experimental system since we do not have measurements of the whole population, just a set of 100 bacilli for each condition. The rounds of cutting typically-varied between 0 and 150 iterations, depending on how many cuts the constraints of each model permits. Model rules we attempted included: cutting chains randomly, cutting chains randomly above a certain length threshold (7,5 or 3 cells per chain minimum), cutting chains in half, and cutting chains to make daughters a minimum length (3 cells,4 cells, or draw from set of values averaging ~ 3 cells per chain) (Fig. S7).

Supplementary Material

Refer to Web version on PubMed Central for supplementary material.

Acknowledgments

The authors wish to thank members of the Schneewind and Missiakas laboratories for discussions. This work was supported by a grant from the National Institute of Allergy and Infectious Diseases (NIAID), Infectious Diseases Branch (AI69227) to O.S. V.J.A and J.W.K. acknowledge support from the Biodefense Training Grant in Host-Pathogen Interactions (AI065382) and the Molecular Cell Biology Training Grant (GM007183), respectively. The authors acknowledge membership within and support from the Region V 'Great Lakes' Regional Center of Excellence in Biodefense and Emerging Infectious Diseases Consortium (GLRCE, NIAID Award 1-U54-AI-057153).

References

Abramoff M, Magelhaes P, Ram S. Image processing with ImageJ. Biophotonics International. 2004; 11:36–42.

Ahn JS, Chandramohan L, Liou LE, Bayles KW. Characterization of CidR-mediated regulation in *Bacillus anthracis* reveals a previously undetected role of S-layer proteins as murein hydrolases. Mol Microbiol. 2006; 62:1158–1169. [PubMed: 17005012]

Allman R, Hann AC, Manchee R, Lloyd D. Characterization of bacteria by multiparameter flow cytometry. J Appl Bacteriol. 1992; 73:438–444. [PubMed: 1447060]

Baba T, Schneewind O. Targeting of muralytic enzymes to the cell division site of Gram-positive bacteria: repeat domains direct autolysin to the equatorial surface ring of *Staphylococcus aureus*. EMBO J. 1998; 17:4639–4646. [PubMed: 9707423]

Bendtsen JD, Nielsen H, von Heijne G, Brunak S. Improved prediction of signal peptides: SignalP 3.0. J Mol Biol. 2004; 340:783–795. [PubMed: 15223320]

Bouvier T, Troussellier M, Anzil A, Courties C, Servais P. Using light scatter signal to estimate bacterial biovolume by flow cytometry. Cytometry. 2001; 44:188–194. [PubMed: 11429769]

Bruckner V, Kovacs J, Denes G. Structure of poly-D-glutamic acid isolated from capsulated strains of *B. anthracis*. Nature. 1953; 172:508. [PubMed: 13099252]

Buist G, Kok J, Leenhouts KJ, Dabrowska M, Venema G, Haandrikman AJ. Molecular cloning and nucleotide sequence of the gene encoding the major peptidoglycan hydrolase of *Lactococcus lactis*, a muramidase needed for cell separation. J Bacteriol. 1995; 177:1554–1563. [PubMed: 7883712]

Carroll SA, Hain T, Technow U, Darji A, Pashalidis P, Joseph SW, Chakraborty T. Identification and characterization of a peptidoglycan hydrolase, MurA, of *Listeria monocytogenes*, a muramidase needed for cell separation. J Bacteriol. 2003; 185:6801–6808. [PubMed: 14617644]

De Las Rivas B, Garcia JL, Lopez R, Garcia P. Purification and polar localization of pneumococcal LytB, a putative endo-beta-N-acetylglucosaminidase: the chain-dispersing murein hydrolase. J Bacteriol. 2002; 184:4988–5000. [PubMed: 12193614]

Dixon TC, Fadl AA, Koehler TM, Swanson JA, Hanna PC. Early Bacillus anthracis-macrophage interactions: intracellular survival and escape. Cell Microbiol. 2000; 2:453–463. [PubMed: 11207600]

Donnelly MI, Zhou M, Millard CS, Clancy S, Stols L, Eschenfeldt WH, Collart FR, Joachimiak A. An expression vector tailored for large-scale, high-throughput purification of recombinant proteins. Protein Expr Purif. 2006; 47:446–454. [PubMed: 16497515]

Dowd MM, OB, Popham DL. Cortex peptidoglycan lytic activity in germinating *Bacillus anthracis* spores. J Bacteriol. 2008; 190:4541–4548. [PubMed: 18456807]

Finn RD, Mistry J, Tate J, Coggill P, Heger A, Pollington JE, Gavin OL, Gunasekaran P, Ceric G, Forslund K, Holm L, Sonnhammer EL, Eddy SR, Bateman A. The Pfam protein families database. Nucleic Acids Res. 2010; 38:D211–222. [PubMed: 19920124]

Fouet A. The surface of Bacillus anthracis. Molecular Aspects of Medicine. 2009; 30:374–385. [PubMed: 19607856]

Fulford W, Model P. Specificity of translational regulation by two DNA-binding proteins. J Mol Biol. 1984; 173:211–226. [PubMed: 6608587]

Ghuysen JM. Use of bacteriolytic enzymes in determination of wall structure and their role in cell metabolism. Bacteriol Rev. 1968; 32:425–464. [PubMed: 4884715]

Heffron JD, Lambert EA, Sherry N, Popham DL. Contributions of four cortex lytic enzymes to germination of *Bacillus anthracis* spores. J Bacteriol. 2010; 192:763–770. [PubMed: 19966006]

Heffron JD, Orsburn B, Popham DL. Roles of germination-specific lytic enzymes CwlJ and SleB in *Bacillus anthracis*. J Bacteriol. 2009; 191:2237–2247. [PubMed: 19181808]

Heidrich C, Templin MF, Ursinus A, Merdanovic M, Berger J, Schwarz H, de Pedro MA, Holtje JV. Involvement of N-acetylmuramyl-L-alanine amidases in cell separation and antibiotic-induced autolysis of *Escherichia coli*. Mol Microbiol. 2001; 41:167–178. [PubMed: 11454209]

Kajimura J, Fujiwara T, Yamada S, Suzawa Y, Nishida T, Oyamada Y, Hayashi I, Yamagishi J, Komatsuzawa H, Sugai M. Identification and molecular characterization of an N-acetylmuramyl-L-alanine amidase Sle1 involved in cell separation of *Staphylococcus aureus*. Mol Microbiol. 2005; 58:1087–1101. [PubMed: 16262792]

Kern J, Ryan C, Faull K, Schneewind O. *Bacillus anthracis* surface-layer proteins assemble by binding to the secondary cell wall polysaccharide in a manner that requires *csaB* and *tagO*. J Mol Biol. 2010; 401:757–775. [PubMed: 20603129]

Kern JW, Schneewind O. BslA, a pXO1-encoded adhesin of *Bacillus anthracis*. Mol Microbiol. 2008; 68:504–515. [PubMed: 18366441]

Kern JW, Schneewind O. BslA, the S-layer adhesin of *Bacillus anthracis*, is a virulence factor for anthrax pathogenesis. Mol Microbiol. 2009; 75:324–332. [PubMed: 19906175]

Kim HU, Goepfert JM. A sporulation medium for *Bacillus anthracis*. J Appl Bacteriol. 1974; 37:265–267. [PubMed: 4212901]

Koch R. Die Atiologie der Milzbrand-Krankheit, begrundet auf die Entwicklungsgeschichte des *Bacillus anthracis*. Beitrage zur Biologie der Pflanzen. 1876; 2:277–310.

Low LY, Yang C, Perego M, Osterman A, Liddington RC. Structure and lytic activity of a *Bacillus anthracis* prophage endolysin. J Biol Chem. 2005; 280:35433–35439. [PubMed: 16103125]

Marraffini LA, Schneewind O. Targeting proteins to the cell wall of sporulating *Bacillus anthracis*. Mol Microbiol. 2006; 62:1402–1417. [PubMed: 17074072]

Marraffini LA, Schneewind O. Sortase C-mediated anchoring of BasI to the cell wall envelope of *Bacillus anthracis*. J Bacteriol. 2007; 189:6425–6436. [PubMed: 17586639]

Mesnage S, Chau F, Dubost L, Arthur M. Role of *N*-acetylglucosaminidase and *N*-acetylmuramidase activities in *Enterorococcus faecalis* peptidoglycan metabolism. J Biol Chem. 2008; 283:19845–19853. [PubMed: 18490448]

Mesnage S, Fontaine T, Mignot T, Delepierre M, Mock M, Fouet A. Bacterial SLH domain proteins are non-covalently anchored to the cell surface via a conserved mechanism involving wall polysaccharide pyruvylation. EMBO J. 2000; 19:4473–4484. [PubMed: 10970841]

Mesnage S, Fouet A. Plasmid-encoded autolysin in *Bacillus anthracis*: modular structure and catalytic properties. J Bacteriol. 2002; 184:331–334. [PubMed: 11741877]

Mesnage S, Tosi-Couture E, Gounon P, Mock M, Fouet A. The capsule and S-layer: two independent and yet compatible macromolecular structures in *Bacillus anthracis*. J Bacteriol. 1998; 180:52–58. [PubMed: 9422592]

Mignot T, Mesnage S, Couture-Tosi E, Mock M, Fouet A. Developmental switch of S-layer protein synthesis in *Bacillus anthracis*. Mol Microbiol. 2002; 43:1615–1627. [PubMed: 11952909]

Oshida T, Sugai M, Komatsuzawa H, Hong YM, Suginaka H, Tomasz A. A Staphylococcus aureus autolysin that has an N-acetylmuramoyl-L-alanine amidase domain and an endo-beta-N-acetylglucosaminidase domain: cloning, sequence analysis, and characterization. Proc Natl Acad Sci U S A. 1995; 92:285–289. [PubMed: 7816834]

Preisz H. Experimentelle Studien uber Virulenz, Empfänglichkeit und Immunität beim Milzbrand. Zeitschrift für Immunitäts-Forschung. 1909; 5:341–452.

Read TD, Peterson SN, Tourasse N, Baille LW, Paulsen IT, Nelson KE, Tettelin H, Fouts DE, Eisen JA, Gill SR, Holtzapple EK, Okstad OA, Helgason E, Rilstone J, Wu M, Kolonay JF, Beanan MJ, Dodson RJ, Brinkac LM, Gwinn M, DeBoy RT, Madpu R, Daugherty SC, Durkin AS, Haft DH, Nelson WC, Peterson JD, Pop M, Khouri HM, Radune D, Benton JL, Mahamoud Y, Jiang L, Hance IR, Weidman JF, Berry KJ, Plaut RD, Wolf AM, Watkins KL, Nierman WC, Hazen A, Cline RT, Redmond C, Thwaite JE, WHite O, Salzberg SL, Thomason B, Friedlander AM, Koehler TM, Hanna PC, Kolsto AB, Fraser CM. The genome sequence of *Bacillus anthracis* Ames and comparison to closely related bacteria. Nature. 2003; 423:81–86. [PubMed: 12721629]

Ruthel G, Ribot WJ, Bavari S, Hoover T. Time-lapse confocal imaging of development of *Bacillus anthracis* in macrophages. J Infect Dis. 2004; 189:1313–1316. [PubMed: 15031802]

Shockman, GD.; Holtje, J-V. Microbial peptidoglycan (murein) hydrolases. In: Ghuysen, J-M.; Hakenbeck, R., editors. Bacterial Cell Wall. Amsterdam: Elsevier Biochemical Press; 1994. p. 131-166.

Smith TJ, Blackman SA, Foster SJ. Autolysins of *Bacillus subtilis*: multiple enzymes with multiple functions. Microbiology. 2000; 146:249–262. [PubMed: 10708363]

Steen A, Buist G, Horsburgh GJ, Venema G, Kuipers OP, Foster SJ, Kok J. AcmA of *Lactococcus lactis* is an N-acetylglucosaminidase with an optimal number of LysM domains for proper functioning. FEBS Journal. 2005; 272:2854–2868. [PubMed: 15943817]

Sterne M. Avirulent anthrax vaccine. Onderstepoort J Vet Sci Animal Ind. 1937; 21:41–43.

Strominger JL, Ghuysen J-M. Mechanisms of enzymatic bacteriolysis. Science. 1967; 156:213–221. [PubMed: 4960294]

Sugai M, Komatsuzawa H, Akiyama T, Hong YM, Oshida T, Miyake Y, Yamaguchi T, Suginaka H. Identification of endo-b-N-acetylglucosaminidase and N-acetylmuramyl-L-alanine amidase as cluster dispersing enzymes in *Staphylococcus aureus*. J Bacteriol. 1995; 177:1491–1496. [PubMed: 7883705]

Tam C, Glass EM, Anderson DM, Missiakas D. Transposon mutagenesis of *Bacillus anthracis* strain Sterne using *bursa aurealis*. Plasmid. 2006; 56:74–77. [PubMed: 16530833]

Vollmer W, Joris B, Charlier P, Foster S. Bacterial peptidoglycan (murein) hydrolases. FEMS Microbiol Rev. 2008; 32:259–286. [PubMed: 18266855]

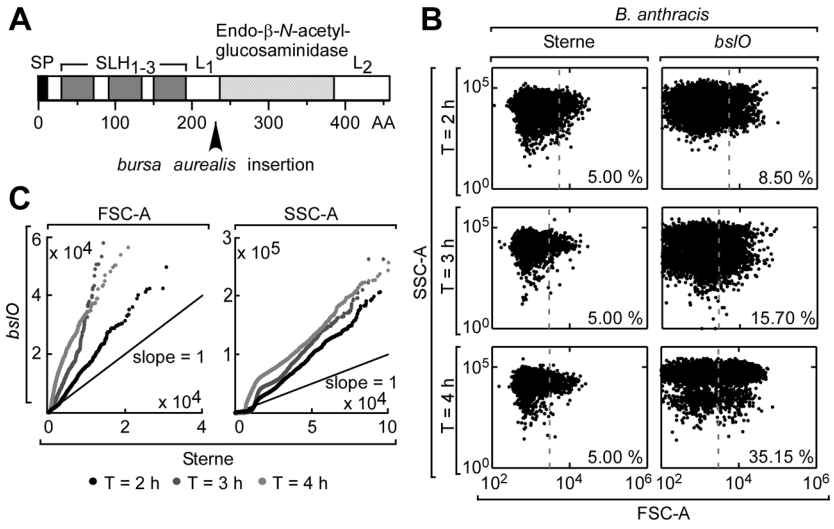

Fig. 1. Isolation of a *B. anthracis bslO* mutant with septum cleavage defect

A. Schematic of the domain organization of the *bslO* open reading frame. The black arrow indicates the size of the truncated translational product expected as a result of *bursa aurealis* insertion in the *bslO* gene. SP, $SLH_{1–3}$, L1 and L2 indicate the BslO signal peptide, surface-layer homology domain triplet and linker region 1 and 2, respectively. The putative enzymatic domain flanked by L1 and L2 is predicted to function as an endo-β-*N*-acetyl-glucosaminidase.

B. Flow cytometry scatter plots of light side-scatter (SSC-A) versus light forward-scatter (FSC-A) of fixed, vegetative *B. anthracis* Sterne (left) or *bslO* mutant (right) cells 2, 3 and 4 h post-germination. Each panel represents events (N = 10,000) gated on values larger than that of a fixed, non-germinated spore population. Gray broken line denotes 95th FSC-A of Sterne population for each time point indicated and the percentages of each population exceeding the Sterne 95th percentile is given in the bottom right of each panel.

C. Scatter plot of magnitude-sorted FSC-A (left) and SSC-A (right) data in A), plotting age-matched *bslO* cohorts against *B. anthracis* Sterne cohorts. (Black: 2 h post-germination; dark gray: 3 h post-germination,; light gray: 4 h post-germination, black line-1:1 unity reference line).

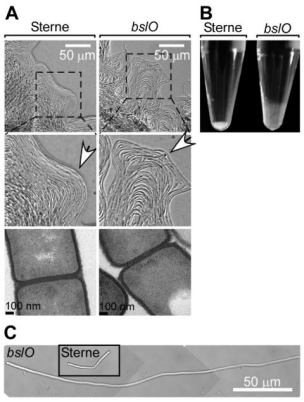

Fig. 2. Morphological phenotypes of *bslO* mutant *B. anthracis*

A. Differential-interference contrast (DIC) micrographs of the edges of a *B. anthracis* Sterne (left) or a *bslO* mutant(right) colony as grown on LB agar (400 × magnification). White arrows on insets point out irregular contours of *bslO* colony margins. Thin-section transmission electron microscopy(TEM)images of *B. anthracis* Sterne (left) and *bslO* mutant bacilli (right) show comparable cell wall and septal architecture.

B. Photograph of culture sediments in eppendorf tubes after centrifugation (18,000 ×*g*) of *B. anthracis* Sterne (left) or *bslO* mutant bacilli (right) grown in LB.

C. DIC micrographs of a *bslO* mutant or *B. anthracis* Sterne (inset) 4 h post-germination in LB.

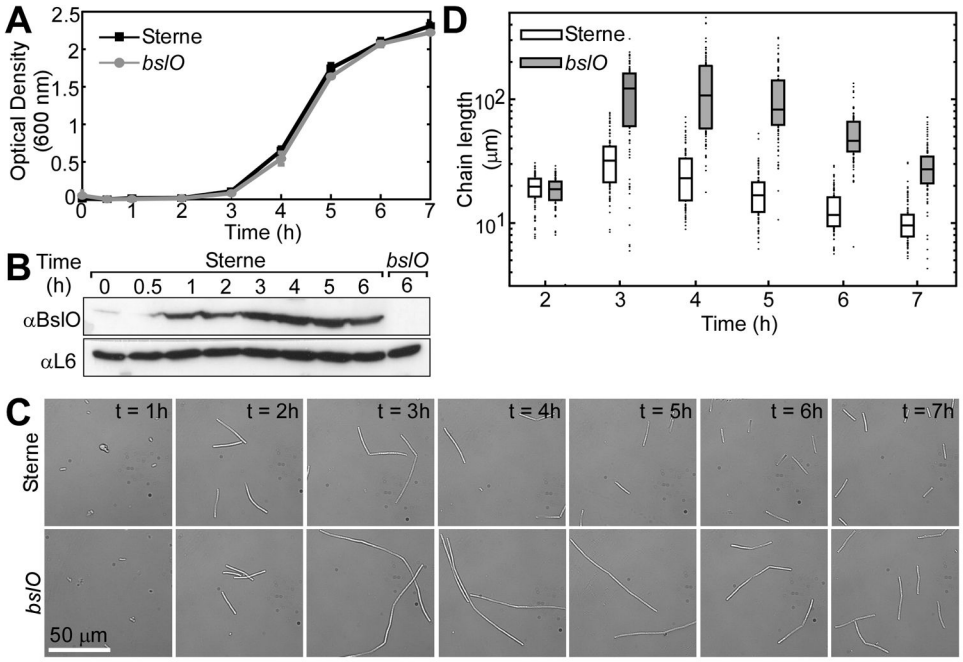

Fig. 3. Role of *bslO* with respect to *B. anthracis* growth phase and chain length

A. Growth curve of *B. anthracis* Sterne (black squares) and its *bslO* mutant (gray circles) germinated in LB at 37 °C as determined by optical density ($Abs_{600\ nm}$). Bars indicate standard deviation ($N = 3$).

B. Immunoblots of total bacterial extracts from mechanically-lysed bacilli probing with polyclonal rabbit antibodies specific for BslO or the ribosomal subunit L6 (loading control).

C. DIC micrographs of vegetative bacilli grown as shown in Panel A and fixed at the indicated time points (1000× magnification).

D. Box and whisker plot of *B. anthracis* Sterne (white) and *bslO* (gray) chain lengths in A (N=100) measured from DIC micrographs as shown in D at indicated time points. Box bounds 25th and 75th percentiles. Black bar denotes sample median and black circles represent first and fourth quartile. Data represents 1 of 3 independent biological replicates.

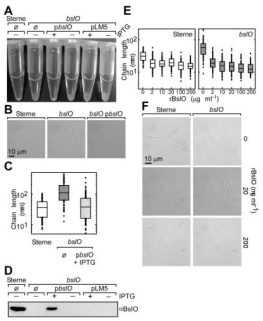

Fig. 4. *Cis* and *trans* complementation of *bslO* mutant bacilli

A. Photograph of culture sediments in eppendorf tubes after centrifugation (18,000 ×*g*) of *B. anthracis* Sterne or *bslO* mutant bacilli transformed with mock (O), plasmid p*bslO* or empty vector control(pLM5). IPTG was added to induce expression of plasmid encoded *bslO*.

B. DIC micrographs of representative *B. anthracis* Sterne, *bslO* and *bslO* (p*bslO*)(+IPTG) bacilli during exponential growth.

C. Box and whisker plot of *B. anthracis* Sterne (white), *bslO* (dark gray) and complemented strain[*bslO* (p*bslO*)] grown in the presence of 1 mM IPTG(lines) chain lengths (*N*=100) measured from DIC micrographs 4 h post-germination. Box bounds 25th and 75th percentiles. Black bar denotes sample median and black circles represent first and fourth quartile. Data represents 1 of 2 independent biological replicates.

D. Immunoblot of total protein preparations of cultures from Panel A with polyclonal rabbit antibodies specific for BslO, verifying the restoration of BslO protein production in the presence of the complementation vector and inducer.

E. Box plots of *bslO* mutant (top) or *B. anthracis* Sterne (bottom) chain lengths(*N*=100) measured from DIC micrographs after treatment with increasing concentrations of recombinant, purified rBslO. Box bounds 25th and 75th percentiles. Black bar denotes sample median and black circles represent first and fourth quartile. Data represents 1 of 2 independent biological replicates.

F. DIC micrographs of vegetative *B. anthracis* Sterne or *blsO* mutant bacilli with or without rBslO treatment (20 or 200 μg·ml^{-1})for 1 hour at 37°C (1000× magnification).

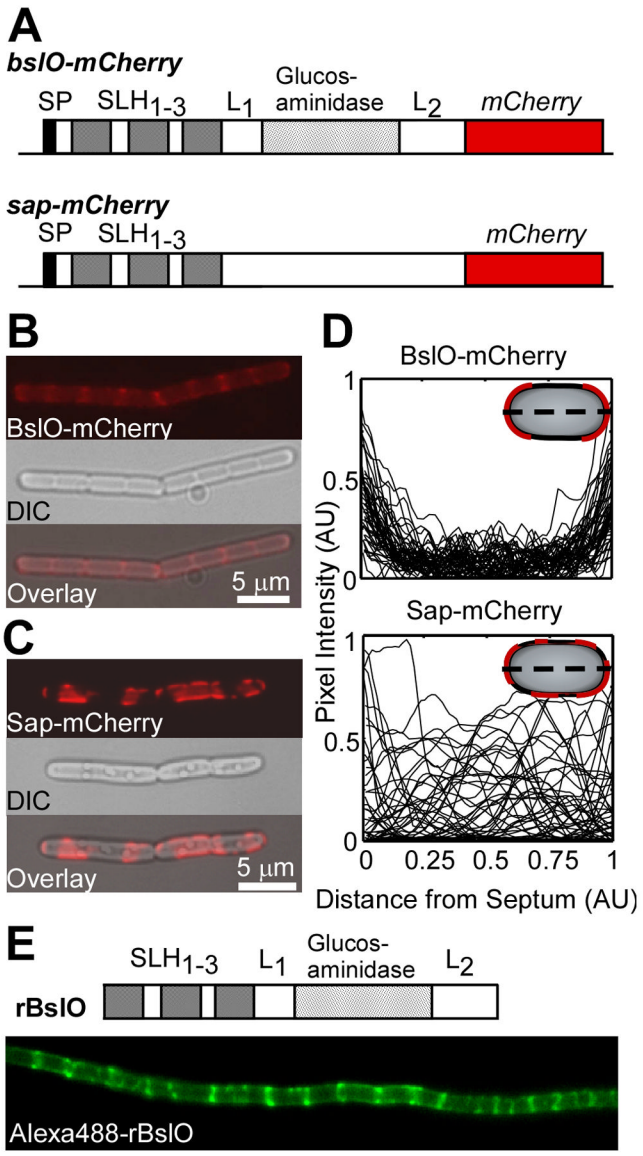

Fig. 5. BslO-mCherry and rBslO localize to cell septa

A. Schematic of the domain organization of *bslO* (top)and the S-layer protein *sap* (bottom) open reading frames as C-terminal translational hybrids to the fluorescent protein (*mcherry*) on the chromosome of *B. anthracis* Sterne.

B,C. Red fluorescence channel (top), DIC (middle) and overlay (bottom) of a representative *bslO-mcherry* (B) and *sap-mcherry* (C) bacillus during exponential growth.

D. Red epifluorescence line plots of intensity normalized (0–1) by the dimmest and brightest pixels observed, respectively. The transects constitute the major axis of individual *bslO-mcherry* (top) or *sap-mcherry* (bottom) cells, normalized (0 to 1)by the length of each cell. Cartoon bacilli (gray ovals) in the upper right depict the position of the intensity transects (broken black line) and representative fluorescent hybrid protein distributions (red).

E. Schematic of the domain organization of rBslO as purified from *E. coli* (top). Micrographs of Alexafluor488-conjugated rBslO incubated with *bslO* bacilli shows that the recombinant protein preferentially localizes to cell septa.

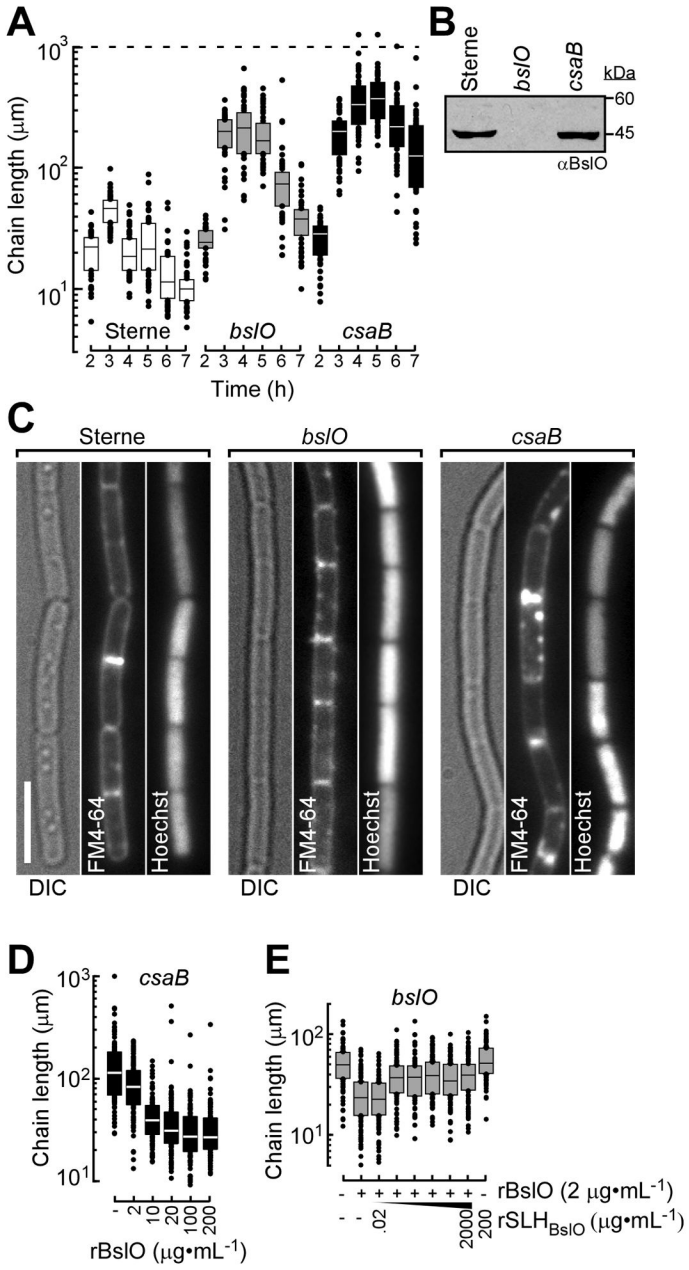

Fig. 6. rBslO activity on *csaB* bacilli

A. box and whisker plot of germinated *B. anthracis* Sterne (white) and *bslO* (gray) or *csaB* mutant bacilli (black) chain lengths (*N*=100) measured from phase micrographs at indicated time points. Box bounds 25th and 75th percentiles. Black bar denotes sample median and black circles represent first and fourth quartile. Data represents 1 of 3 independent biological replicates.

B. Immunoblot of total protein preparations of *B. anthracis* Sterne, *bslO* and *csaB* mutant cultures with polyclonal antibodies specific for BslO, verifying the production of BslO by *csaB* mutant bacilli.

C. Representative DIC and fluorescent micrographs of *B. anthracis* Sterne, *bslO* and *csaB* mutant bacilli stained with Hoechst (DNA/blue) and FM4–64 (membrane/red)to analyze chromosome partitioning and cell separation.

D. Box and whisker plot of *csaB* mutant chain lengths (*N*=100) measured from phase micrographs after 1 h incubation (37 °C) with rBslO at indicated concentrations. Box bounds 25th and 75th percentiles. White bar denotes sample median and black circles represent first and fourth quartile. Data represents 1 of 3 independent biological replicates.
E. Box and whisker plot of *bslO* mutant chain lengths (*N*=100) measured from phase micrographs after 1 h incubation (37°C) with a mixture of rBslO and purifiedSLH_{1-3} − domain of BslO at concentrations indicated. Box bounds 25th and 75th percentiles. Black bar denotes sample median and black circles represent first and fourth quartile. Data represents 1 of 2 independent biological replicates.

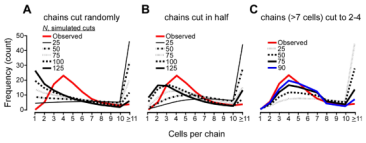

Fig. 7. Simulations of BslO-mediated separation of *B. anthracis* chains

A. Mean curves of cell-per-chain distributions given BslO has an equal probability of cleaving any septum.

B. Mean curves of cell-per-chain distributions given BslO acts on the center-most septum of a randomly-selected chain.

C. Mean curves of cell-per-chain distributions given BslO may only cleave septa of bacilli that are minimally 8 cells per chain in length and only at septa that liberate daughter cells of a minimum length drawn randomly from the set [2,2,3,3,3,4].

The red curve indicates the cell-per-chain distribution of observed chain lengths estimated from 1,000 iterations. The remaining curves are the mean of 10,000 simulations of iterative cleavage events as indicated. The red box shows which cells are candidates for cleavage, given the lengths of the cartoon bacilli. The bracketed chains below indicate all possible outcomes that satisfy each model's rule(s) for cleavage events.

Table 1

Oligonucleotides used in this study

Name	Nucleotide sequence
p*bslO*F	AAAGGTACCATGAAAAAAGTTATTTCTAATGTGTTAGC
p*bslO*R	AAAGGTACCTTATATTTTTAAGTTCTTCTTCAATGTCC
P94	ACACAGGAAACAGCTATGACC
P95	GTTGCTAGTAACATCTGACCG
bslO-mcherry UPF	AAACCCGGGTAGGTGATGGTAAAGGGACATTT
bslO-mcherry UPR	AAAGGTAACTATTTTTAAGTTCTTCTTCAATGTCCA
bslO-mcherry DNF	AAAGGTACCATAAAAAAGGTGTTTTCACTTATGAAAAC
bslO-mcherry DNR	AAAGAATTCAGCCATGGAATTAATACGACG
P283	TTTGGTACCAGCAAGGGCGAGGAGG
P284	TTTGGTACCTTACTTGTACAGCTCGTCCATG
P293	TTTCCCGGGAAAAACAGTTGAAATTGAAGCTTTC
P294	TTTGGTACCTTTTGTTGCAGGTTTTGCTTC
P303	TTTGGTACCTTAAAAATCATTTAATAAATGATTAATAAGGG
P304	TTTGAATTCAGGCTGAGCATTTTCATCAACT
bslO $_{SLH}$F	GGAATTCCATATGGTCGCACTTCAAGTAGTGATGG
bslO $_{SLH}$*R*	AAACTCGAGTGCATATTCTTCACGTGTTAAAACA
bslO-LICF	TACTTCCAATCCAATGCTTCTTACAAAAGAATTTCCAGACGTTC
bslO-LICR	TTATCCACTTCCAATGTTATATTTTTAAGTTCTTCTTCAATGTCCA